Bump'em: an Open-Source, Bump-Emulation System for Studying Human Balance and Gait

Guan Rong Tan[†], Michael Raitor[†], and Steven H. Collins^{*}

Abstract—Fall-related injury is a significant health problem on a global scale and is expected to grow with the aging population. Laboratory-based perturbation systems have the capability of simulating various modes of fall-inducing perturbations in a repeatable way. These systems enable fundamental research on human gait and balance and facilitate the development of devices to assist human balance. We present a robotic, rope-driven system capable of rendering bumps and force-fields at a person's pelvis in any direction in the transverse plane with forces up to 200 N, and a 90% rise time of as little as 44 ms, which is faster than a human's ability to sense and respond to the force. These capabilities enable experiments that require stabilizing or destabilizing subjects as they stand or walk on a treadmill. To facilitate use by researchers from all backgrounds, we designed both a configuration with simpler open-loop force control, and another with higher-performance, closed-loop force control. Both configurations are modular, and the open-loop system is made entirely from 3D-printed and catalog components. The design files and assembly instructions for both are freely available in an online repository.

I. INTRODUCTION

Falls are a significant medical problem facing society. One in three older adults [1] and one in two people with amputations [2] fall each year. Falls often lead to serious injury or death [3] and cost the U.S. healthcare system approximately \$50 billion USD annually [4]. Improved understanding of falls and better fall-prevention technology could benefit millions of people.

In order to prevent falls, we need tools to identify the specific mechanisms through which they occur. External bumps and internally generated errors resulting in undesirable center of mass (COM) movement account for about half of falls [5]. Emulating real-world fall conditions while in a laboratory setting enables researchers to safely and repeatably study underlying mechanisms and methods to prevent falls. The prevalence of COM-related falls and benefits of studying falls in a laboratory setting motivate the development of laboratory-based perturbation systems to study COM-related falls.

We identified three key design features to make a laboratory-based perturbation system as useful as possible: versatility, responsiveness, and ease-of-access.

*This material is based upon work supported by the National Science Foundation under Grant No. IIS-1527140 and CMMI-1734449, and the National Science Foundation Graduate Research Fellowship under Grant No. DGE-1656518.

Department of Mechanical Engineering, Stanford University

A perturbation system should be versatile and allow the experimenter a high level of control over the disturbance profile. The system should be able to perturb a participant from multiple directions, for example, to study differences in stability in the medial-lateral and anterior-posterior directions [6]. The ability to generate force profiles of different shapes and magnitudes is also important, as it allows the experimenter to emulate different types of disturbances. The system should also be able to apply sufficient force. To counteract the horizontal ground reaction forces generated by a 70 kg person while walking, for example, a perturbation system must be able to apply forces of approximately 170 N [7]. In addition to displaying force when desired, the device should be able to avoid applying undesired forces so that subjects can move freely while standing or walking on a treadmill.

The system should be as fast as possible to render any force desired by the experimenter. We estimate the time to reach 90% of the peak force from bumping into a stiff object with the pelvis at a typical walking speed to be approximately 20 -45 ms [8]. In order to accurately render a perturbation by a stiff object, the system should have a 0-90% rise time in that range. The human response is another important aspect of the system. Human response time for visual, auditory, and haptic cues are 180 ms, 140 ms, and 140 ms, respectively [9]. Subcortical responses are faster, and a model of stretch-reflex delays estimates the response time in humans to be 90 ms [10]. Using this model with more conservative estimates of nerve lengths suggests a $60\,\mathrm{ms}$ response time. To unexpectedly perturb a subject, the system must be fast enough to display a significant amount of force in less time than it takes to respond to a stimulus. These data suggest that 45 ms and 60 ms are important benchmarks for responsiveness.

Providing the research community with a financially and technically accessible research tool would enable more widespread studies on falls. There are many existing perturbation systems that have high functionality, but are specialized and would be difficult to replicate. An accessible, open-source design should be low-cost, made entirely of 3D-printed and catalog components, and come with instructions for component purchase, assembly and control. These features would allow the system to be built and used by any researcher regardless of their level of technical expertise and would avoid future researchers having to design and build their own system for a specific experiment.

Physical perturbation systems have been useful in previous studies of standing and walking balance by unexpectedly bumping participants. These perturbation systems used a

[†]These authors contributed equally to this work.

^{*}Corresponding Author: S. H. Collins, 452 Escondido Mall, Stanford, CA 94305, USA. Email: stevecollins@stanford.edu

variety of strategies to create a perturbation, including dropping weights attached to the subject via ropes [11]-[13], pushing them with rigid mechanisms [14]-[18], tugging them with rope pulling mechanisms [19]-[23], or even manually pushing or pulling them [24], [25]. Analyzing the different strengths of these systems indicates that a modular, motor-driven rope system with a simple transmission could provide the desired versatility, responsiveness, and accessibility. Modular systems can be reconfigured for a variety of experiments, motor-driven systems can display various force profiles, and rope-based systems minimally restrict subject movement. All of these attributes contribute to the versatility of the system. Using high-stiffness ropes enables higher responsiveness, and a simple, motor-driven transmission makes the system technically and financially accessible.

In this paper, we present a modular perturbation system, where each module has an independently controlled motor that can apply forces in a single direction with a rope. It is capable of perturbing a standing or walking subject at the hip with various force profiles, magnitudes of up to 200 N and a rise time as little as 44 ms. We also demonstrate how modules can be used cooperatively to emulate perturbations in any direction in the transverse plane, and can be paired with optional encoders to render force-fields. By providing this research tool to the rehabilitation robotics and biomechanics communities, we hope to enable researchers to improve the collective understanding of how falls occur, how to prevent them, and how humans move in novel environments.

II. SYSTEM DESIGN

We designed two configurations of the perturbation system: one performs *open-loop* force control, and is the simplest and least-expensive configuration of the system. The other includes an additional force sensor that enables it to perform *closed-loop* force control, which improves tracking performance in general and especially when larger hip motions are expected, such as when the subject is walking. In this section, we first describe an overview of the physical system architecture, followed by the system modelling we performed to inform the selection of various design components. We then describe the mechanical design, sensor setup and controller design. Finally, we describe features of the open-source design that make the system components easy to acquire, assemble, and use.

A. System Overview

The perturbation system is modular. Each module pulls in a single direction, and multiple independently-controlled modules can be set up based on the number of pull directions needed. Fig. 1A depicts the layout of a four-module system that allows application of forces in any direction. The modules can be placed at hip height to apply perturbations in the transverse plane. Each module has a motor unit controlled by a control unit. A stiff rope is wound around a reel drum in the motor unit and attached to a harness worn by the subject on the other end. A safety breakaway cable that breaks within

a specified force range and a force sensor are attached in series with the rope. The force sensor is only required in the closed-loop configuration.

B. System Modelling

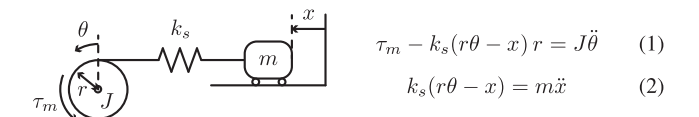


Fig. 2. Simplified model of the human-robot system.

We built a dynamical model of the transmission components which allowed us to identify the motor specifications, reel drum radius, and rope characteristics that would achieve desired step response rise times.

We model the transmission as a mass-spring system (Fig. 2), where the subject is a frictionless sliding mass m with displacement x. The mass is attached to a rope that is modeled as a spring with spring constant k_s . This rope is attached to a drive train with combined rotational inertia J, radius r, applied torque τ_m , and angular displacement θ .

From this model, we derived the equations of motion. We estimate the rope force as $k_s(r\theta-x)$. We assumed an ideal bang-bang controller that applied maximum, then minimum motor currents allowable given the motor specifications and voltage limitations from the instantaneous motor velocity. We then iteratively solved for the step timings that would achieve our targeted force with minimum rise time and zero overshoot. We obtained the minimum rise times for various sets of motor, reel drum and rope parameters. Faster rise times were achieved with shorter and stiffer ropes. Hence, modules were placed as close as possible to the subject while allowing a desired range of motion. The ropes in our setup are approximately 4.5 ft. We also selected a motor that could achieve our desired rise times without a gearbox or a large reel drum that would increase system cost and size.

Since this simulation assumed an ideal controller and a frictionless system, we expect the real system to perform slightly worse. Hence, we selected a motor and reel drum radius that could outperform the 60 ms rise time goal. We selected a 260 W maxon brushless motor (EC-90 Flat, maxon Group, Switzerland) and reel drum radius of 0.75 in, which could achieve rise times of 30.1 ms in simulation.

C. Mechanical Design

Each module comprises a harness, rope, breakaway cable, motor unit, control unit and optional sensors. The subject wears a hip harness with ropes attached that transmit the perturbation forces from the motor unit to the subject. A breakaway cable is tied in series with the rope, acting as a mechanical fuse designed to fail at 250 N to ensure the subject does not experience unsafe force magnitudes. A force sensor is also placed in series with the rope to measure the tensile forces being applied, and is only needed for the closed-loop configuration.

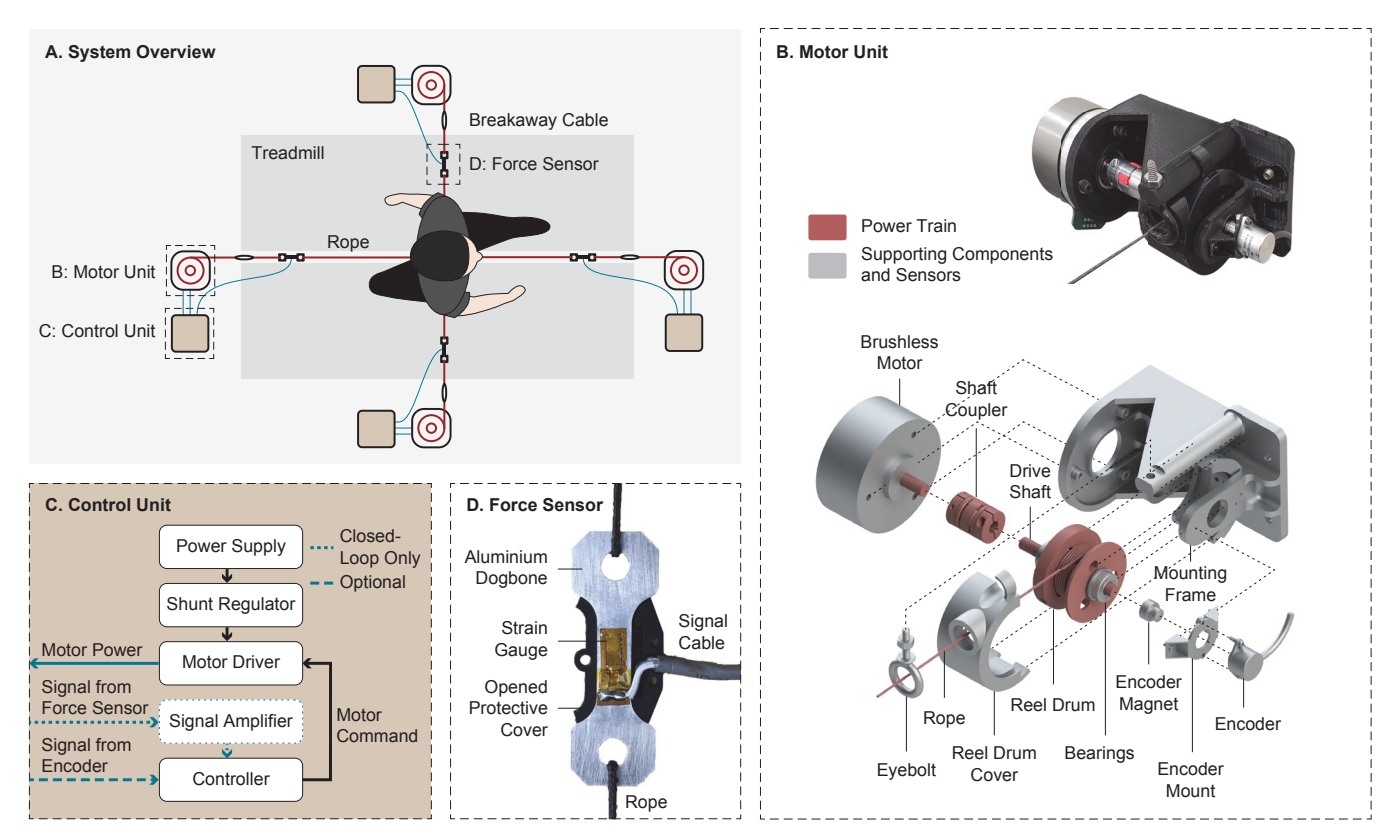


Fig. 1. Physical System Architecture. (A) Overhead Schematic of a four-module configuration. Breakaway cable and force sensors are placed in series with each rope that links the subject to the motor unit and its respective control unit. (B) Real and exploded view of the motor unit. (C) Components within the control unit that control power and signal flow to the motor unit. (D) Force sensor used to measure rope force.

The motor unit (Fig. 1B) is responsible for applying forces to the rope. Within the motor unit, the rope is guided through an eyebolt and wound tightly around a reel drum. The rope should pass through the center of the eyebolt, but if a subject moves too much, the eyebolt prevents the rope from getting pulled over the side of the reel drum. A cover is placed around the reel drum and helps keep the rope in place in case any slack is generated during fast spooling and unspooling. The reel drum comprises a 3D-printed drum that is bolted to a flanged shaft coupler that clamps onto the drive shaft. The drive shaft is supported on both sides by radial bearings. An optional magnetic encoder can be mounted to one end if state-based control if desired, but is otherwise unnecessary for either the open-loop or closed-loop configurations. A shaft coupler connects the drive shaft to the motor shaft of the brushless motor. These components are all held together by a 3D-printed mounting frame designed to sustain the loading forces expected. Strengthening ribs run along the main body, support arms for the drive shaft bearings, and eyebolt mount. These features are designed to be robust against the tensile, torsional and bending loads expected. This frame has mounting holes that allow it to be mounted to an 80/20 (IN, USA) frame or directly to a wall at hip height.

The control unit (Fig. 1C) controls the power and signal flow to the motor unit. The motor is driven by a motor

driver (ESCON 70/10, maxon Group, Switzerland) that is powered by a 48V DC power supply (RSP200048, MEAN WELL, Taiwan). A shunt regulator (DRS 70/30, maxon Group, Switzerland) is placed in series to dissipate the excess current generated during braking. A controller converts the experimenter's desired force commands to the motor driver via a single analog output. The driver will command current corresponding to approximately 40 N continuously and up to 200 N periodically. If the optional encoder is included, its signals are passed to the controller through an analog input. In the closed-loop configuration, signals from the force sensor are processed by a signal amplifier (IAA100, Futek, CA, USA) and passed to the controller via a second analog input. In our system, we used a Speedgoat real-time controller (Speedgoat, MA, USA) running at 1000 Hz.

D. Sensors

In the closed-loop configuration, we measure the applied forces in order to improve tracking performance. The forces are measured by a force sensor placed in series with the rope. In each force sensor, two strain gauges (SGD-7/1000-LY13, Omega, CT, USA) are placed on opposite sides of a thin aluminum dogbone and wired in series with each other. They are connected to form a quarter of a wheatstone bridge circuit that is mounted near the module. This configuration will exclude readings due to any bending forces generated

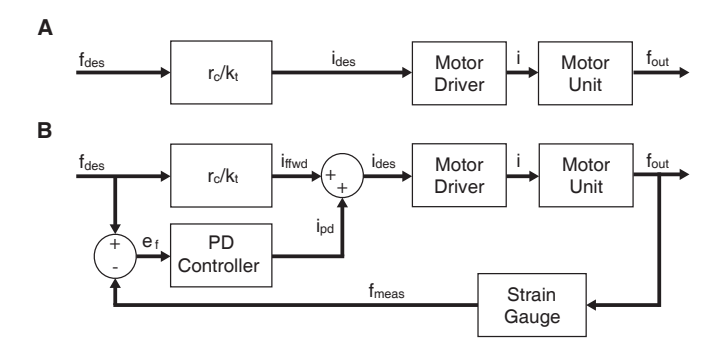


Fig. 3. Control Block Diagrams (A) Open-loop force control (B) Closed-loop force control with force feedback

on the aluminum dogbone.

An optional magnetic encoder can also be used to collect data on the angular displacement of the drive shaft. This enables implementation of state-based control to render virtual environments such as force-fields. The encoder magnet (RMA37A3, Renishaw, United Kingdom) is clamped directly to the shaft, and the encoder (RM22, Renishaw, United Kingdom) is mounted on a 3D printed mount that is attached to the mounting frame. Both the force sensor and motor encoder signals are filtered with a 2nd order Butterworth filter with a cutoff frequency of $60\,\mathrm{Hz}$.

E. Controller

We developed two controllers, one open-loop and one closed-loop. The open-loop controller is the simplest to use, as it commands a constant current based on desired force and a simplified system model. Bang-bang control can be used in the open-loop configuration, but is difficult to tune. For ease-of-use by other researchers, we opted for the simple model-based control described below for the open-loop option. The closed-loop controller is expected to offer improved performance, as it uses a feedback term on measured force, which requires the use of a force sensor.

The open-loop controller sets motor current as

$$i_{des} = f_{des} r / k_t, \tag{3}$$

where i_{des} is the desired current command sent to the motor driver, f_{des} is the desired force, r is the reel drum radius, and k_t is the torque constant of the motor. This model does not account for transmission inertia, which affects force transmitted to the rope during periods of acceleration.

In addition to the desired force, f_{des} , the closed-loop controller uses measured force, f_{meas} , and their respective time derivatives, \dot{f}_{des} and \dot{f}_{meas} . The tuning parameters k_p and k_d are the proportional and derivative gains, respectively.

$$i_{des} = k_p (f_{des} - f_{meas}) + k_d (\dot{f}_{des} - \dot{f}_{meas}) + f_{des} r/k_t$$
 (4)

The \dot{f}_{meas} term was calculated using a noise-suppressing numerical differentiation method that averages the derivative of the measured force over the previous three time steps, as described in [26].

System Costs

Components	Single-Module System	Per Additional Module
Open-Loop w/o Encoder	\$1,718	\$1,490
Closed-Loop w/o Encoder	\$2,389	\$1,947
Encoder	\$91	\$82

TABLE I: Cost of different system combinations in USD.

F. Open-Source Design

We designed our modules to be easy for others to replicate. The open-loop configuration is constructed entirely from 3Dprinted or catalog components. The reel drum, reel drum covers, encoder mount and mounting frame are made from 3D-printed Polylactic Acid (PLA). We provide the CAD models in the accompanying repository. The brushless motor, motor driver, shunt regulator, power supply, signal amplifier, strain gauge, encoder and other mechanical components are catalog parts. We provide a bill of materials for all these components. For the closed-loop module, the aluminum dogbone can be ordered from Proto Labs (MN, USA). We provide the CAD models in the accompanying repository. The components in the strain gauge wheatstone bridge circuitry are catalog parts, but require some soldering to be assembled, and we provide schematics and photos for how to do so. A complete bill of materials, all design files, and assembly instructions for the system are freely available at https://biomechatronics.stanford.edu/bump-em, where we also intend to post future versions of the system.

We designed the system to be modular, so that it could be easily configured for a variety of experimental needs. The number of modules and positioning of each in the lab can be chosen depending on the range of pull directions needed.

We designed the system to be inexpensive. A system with a single module, excluding the optional encoder, costs \$1,718 for the open-loop and \$2,389 for the closed-loop configuration. Some items, such as the subject harness, are baseline costs that do not scale with number of modules. Table I lists the cost of a single-module system, which includes baseline costs, and the cost of additional modules for both open-loop and closed-loop configurations.

We do not include the controller in the listed costs due to the wide range of options. The system only requires 0-5 V analog inputs and outputs from the controller. Hence, one can use anything from open-source microcontrollers such as Arduino (Arduino, MA, USA) to larger real-time systems such as Speedgoat (Speedgoat, MA, USA).

III. EXPERIMENTAL TESTS OF PERFORMANCE

We tested the system with one participant (N=1; male; 70 kg; 1.8 m; 24 yrs) in order to determine how well the different system configurations would perform as the human responded to perturbations.

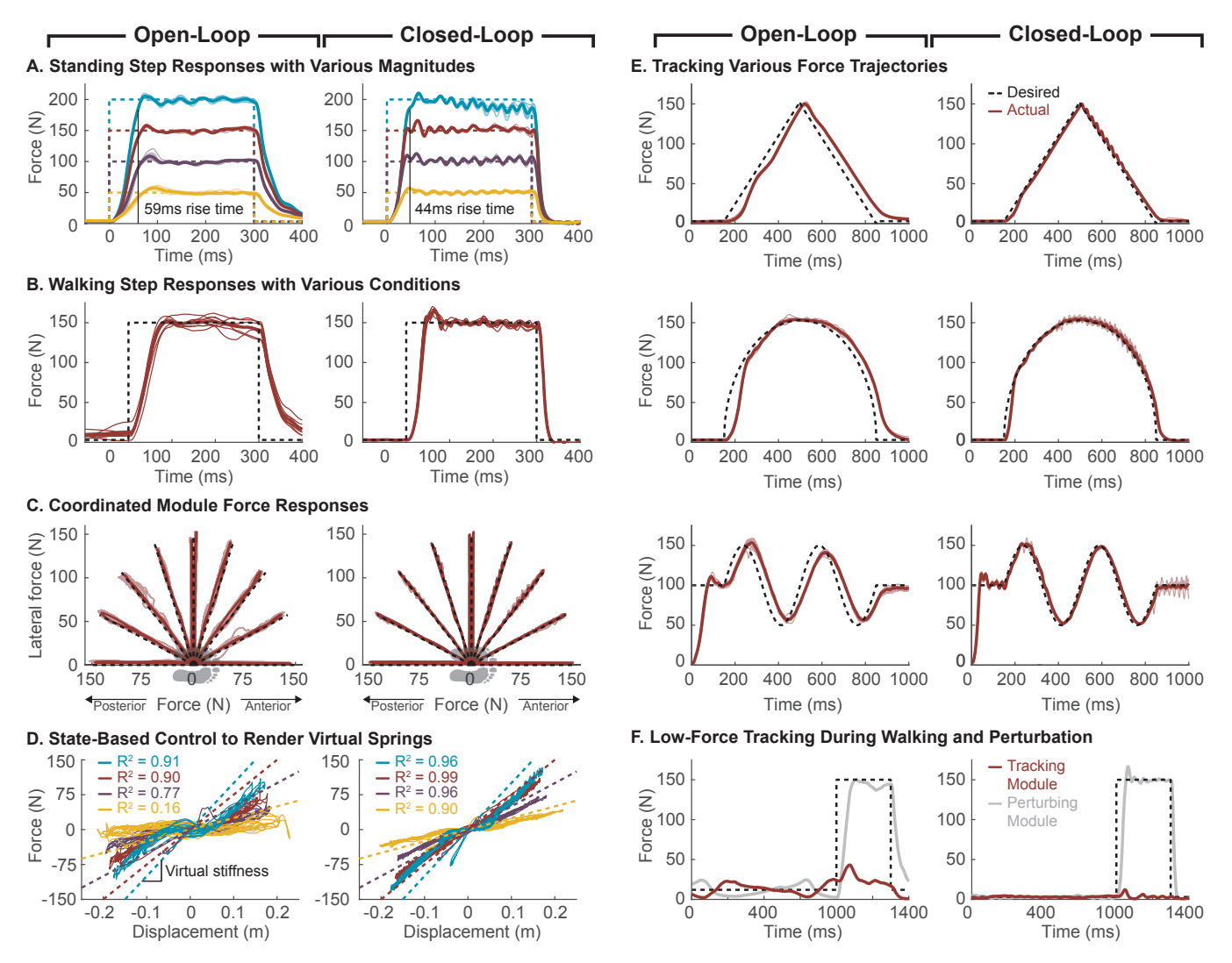


Fig. 4. Force-tracking results using open-loop (left) and closed-loop (right) system configurations (**A**) Step responses applied in the lateral direction with magnitudes of 50, 100, 150 and 200 N while standing. Thin lines represent 10 individual trials for each magnitude. Thick lines represent mean trajectories. Dashed lines represent desired force. (**B**) Step responses while walking with perturbations in the medial, lateral, anterior, and posterior directions during early (10%) and mid-late (65%) swing phase. Thin lines represent mean of 10 trials for each condition. Thick line represents mean of all trials across conditions. (**C**) Tracking performance of combined perturbations using a module positioned in the lateral and either anterior or posterior directions. Thin lines represent individual trials. Thick lines represent mean of 10 trials. Desired trajectories are offset by 22.5 deg. (**D**) Net force-displacement curves while rendering 250, 500, 750, and 1000 N m⁻¹ spring stiffnesses shown in yellow, purple, red, and blue, respectively. (**E**) Force-trajectory tracking plots for a ramp, semi-circle, and sinusoid offset to 100 N. (**F**) Low-force tracking of anterior module during walking while posterior module applies a perturbation. Red lines indicate motor module tracking a low-force command (12 N for open-loop and 3 N for closed-loop). Grey lines indicate force from perturbing motor module. Dashed line indicates desired perturbation force.

A. Standing Step Responses with Various Magnitudes

We measured peak force and rise time using step responses. We performed perturbations in the lateral direction while standing with magnitudes of 50, 100, 150, and 200 N with 10 trials for each magnitude (Fig. 4A). The $200\,\mathrm{N}$ responses were slowest of all magnitudes and had a 0-90% rise time of 59 ± 1.0 ms for the open-loop configuration and 44 ± 0.7 ms for the closed-loop configuration.

B. Walking Step Responses with Various Conditions

We tested $150\,\mathrm{N}$ step responses in different directions and times in the gait cycle during walking. They were displayed in anterior, posterior, medial, and lateral directions during early (10%) and mid-late (65%) swing phase. We found the open-loop configuration to be relatively fast and consistent, with a 0-90% rise time of 66 ± 6.4 ms. We found the closed-loop configuration to be faster and more consistent with a rise time of 41 ± 2.7 ms.

C. Coordinated Module Force Responses

We simultaneously applied force with two modules positioned to the left and to the front or rear of a standing subject. Each module tracked a ramp-like force profile lasting 700 ms, similar to that shown in the top row of Fig. 4E. Each module provided either the medial-lateral or anterior-posterior components of 9 force vectors in the transverse plane. (Fig. 4C). We tracked resulting force vectors with an average RMS error of 13.8 N for open-loop and 5.2 N for closed-loop.

D. State-Based Control to Render Virtual Springs

We used the optional encoder on the drive shaft to provide estimates of subject displacement from a set point. We applied motor commands to simulate a virtual spring force with spring constants of $250\,,\,500\,,\,750\,,$ and $1000\,\mathrm{N\,m^{-1}}$ (Fig. 4D). Linear fits to the data (with intercepts forced through the origin) have slopes of $39\,,\,192\,,\,345\,,$ and $460\,\mathrm{N\,m^{-1}}$ with R^2 of 0.16, 0.77, 0.90, and 0.91, respectively, for the open-loop configuration and $174\,,\,376\,,\,609\,,$ and $660\,\mathrm{N\,m^{-1}}$ with R^2 of 0.90, 0.96, 0.99, and 0.96, respectively, for the closed-loop configuration.

E. Tracking Various Force Trajectories

We tested ramp, semi-circle, and sinusoid force trajectories on a standing participant in order to test the system's ability to track various force trajectories. Each trajectory was performed 10 times. The RMS error for all trials of each trajectory was 13.5, 18.8, and $25.0\,\mathrm{N}$, respectively, for the open-loop configuration, and 4.9, 8.6, and $16.1\,\mathrm{N}$, respectively, for the closed-loop configuration.

F. Low-Force Tracking During Walking and Perturbation

We tested the system's ability to minimize rope slack using low-force tracking, as slack adversely affects perturbation magnitude and timing consistency. We used a low-force tracking magnitude of $12\,\mathrm{N}$ for the open-loop configuration and $3\,\mathrm{N}$ for the closed-loop configuration in the anterior direction with a perturbation from the posterior module during walking (Fig. 4F). These directions were chosen as they performed worst during pilot testing. The open-loop configuration tracked the low-force command with a RMS error of $9.8\,\mathrm{N}$ and the closed-loop configuration tracked it with a RMS error of $1.6\,\mathrm{N}$.

IV. DISCUSSION

Both open-loop and closed-loop configurations perform well according to our design criteria. They both produce enough force, respond quickly, and are made from simple, easy-to-make modules. Both configurations are versatile enough to perturb participants during standing or walking, display force in any direction by coordinating modules, and can be combined with optional sensors to render force-fields. The force-field rendering is adequate, especially in the closed-loop configuration with stiffer virtual springs.

Both system configurations are highly responsive. Stepresponses to $200\,\mathrm{N}$ during standing demonstrated rise times

of 59 ms for the open-loop configuration and 44 ms for the closed-loop configuration. The open-loop configuration meets the requirement to beat the human stretch-reflex in order to perturb a subject before they sense and respond to the onset of perturbation. The closed-loop configuration is faster than the human stretch-reflex, and is approaching the rise-time required to accurately render contact with stiff objects. The active force control of the system allows it to successfully track a variety of force profiles with high accuracy. The closed-loop configuration performs slightly better across all force-tracking tasks, and the improved performance is most notable during walking. The closed-loop step response drops slightly at the end of the 200 N standing perturbation because the subject adopted a less-stable pose and consequently accelerated more when perturbed, thus requiring the motor to rotate with higher velocity, generate larger back-emf, and produce slightly lower force. This result indicates that changes in a subject's impedance affects system dynamics.

The higher performance of the closed-loop configuration make it preferable if the additional complexity and cost of the force sensor and associated circuitry are manageable. The closed-loop configuration has faster rise times, better force tracking, and performs effective low-force tracking between perturbations that makes it almost imperceptible during walking. The open-loop configuration performs well enough for many experiments and if low-force tracking performance during walking is problematic for an experiment, slack could be left in the ropes, at the cost of consistency in perturbation timing and magnitude.

V. CONCLUSION

In this paper, we provide the design and characterization of a modular, open-source perturbation system that can be made entirely out of affordable catalog and 3D-printed components. The modularity of this system makes it useful in a wide range of experiments. The simple design using easily-obtained components makes the system financially and technically accessible and therefore easy to replicate. The system is capable of perturbing subjects with forces of up to 200 N in any direction at the hips, fast enough to display 90% of the desired force before a subject can detect and respond to it, and capable of rendering force-field environments with the use of optional encoders. We provide two versions of the system: an open-loop configuration which is less expensive, simpler to assemble, and suitable for applications requiring less-precise force control, and a closed-loop configuration which is approximately 30-40% more expensive depending on the number of modules in the system, requires assembly of additional sensors, and provides better force tracking, especially during high-movement activities. Both system configurations can serve as useful research tools that will enable researchers from all backgrounds to study how falls occur, how to prevent them, and how humans move in novel environments.

REFERENCES

- J. M. Hausdorff, D. A. Rios, and H. K. Edelberg, "Gait variability and fall risk in community-living older adults: A 1-year prospective study," *Archives of Physical Medicine and Rehabilitation*, vol. 82, no. 8, pp. 1050–1056, 2001.
- [2] W. C. Miller, M. Speechley, and B. Deathe, "The prevalence and risk factors of falling and fear of falling among lower extremity amputees," *Archives of Physical Medicine and Rehabilitation*, vol. 82, no. 8, pp. 1031–1037, 2001.
- [3] A. M. Dellinger and J. A. Stevens, "The injury problem among older adults: Mortality, morbidity and costs," *Journal of Safety Research*, vol. 37, no. 5, pp. 519–522, 2006.
- [4] C. S. Florence, G. Bergen, A. Atherly, E. Burns, J. Stevens, and C. Drake, "Medical costs of fatal and nonfatal falls in older adults," *Journal of the American Geriatrics Society*, vol. 66, no. 4, pp. 693–698, 2018. [Online]. Available: https://onlinelibrary.wiley.com/ doi/abs/10.1111/jgs.15304
- [5] S. N. Robinovitch, F. Feldman, Y. Yang, R. Schonnop, P. M. Leung, T. Sarraf, J. Sims-Gould, and M. Loughin, "Video capture of the circumstances of falls in elderly people residing in long-term care: an observational study," *The Lancet*, vol. 381, no. 9860, pp. 47 54, 2013. [Online]. Available: http://www.sciencedirect.com/science/article/pii/S014067361261263X
- [6] S. M. O'Connor and A. D. Kuo, "Direction-dependent control of balance during walking and standing," *Journal of neurophysiology*, vol. 102, no. 3, pp. 1411–1419, 2009.
- [7] M. Kuster, S. Sakurai, and G. Wood, "Kinematic and kinetic comparison of downhill and level walking," *Clinical Biomechanics*, vol. 10, no. 2, pp. 79–84, 1995.
- [8] A. C. Laing, I. Tootoonchi, P. A. Hulme, and S. N. Robinovitch, "Effect of compliant flooring on impact force during falls on the hip," *Journal of Orthopaedic Research*, vol. 24, no. 7, pp. 1405–1411, 2006. [Online]. Available: http://doi.wiley.com/10.1002/jor.20172
- [9] R. S. Woodworth and H. Schlosberg, "Experimental psychology, (rev. ed.)," 1954.
- [10] H. L. More and J. M. Donelan, "Scaling of sensorimotor delays in terrestrial mammals," *Proceedings of the Royal Society B: Biological Sciences*, vol. 285, no. 1885, p. 20180613, 2018. [Online]. Available: https://royalsocietypublishing.org/doi/10.1098/rspb.2018.0613
- [11] J. M. Chandler, P. W. Duncan, and S. A. Studenski, "Balance Performance on the Postural Stress Test: Comparison of Young Adults, Healthy Elderly, and Fallers," *Physical Therapy*, vol. 70, no. 7, pp. 410–415, 1990. [Online]. Available: https://academic.oup.com/ptj/article/2728657/Balance
- [12] A. Gildenhuys, P. Zandiyeh, G. Kuntze, P. Goldsmith, and J. L. Ronsky, "Biomechanical Analysis of a Dynamic Stability Test System to Evoke Sway and Step Recovery," *Journal of Biomechanical Engineering*, vol. 137, no. 10, p. 104501, 2015. [Online]. Available: http://biomechanical.asmedigitalcollection.asme. org/article.aspx?doi=10.1115/1.4031329
- [13] C. W. Luchies, N. B. Alexander, A. B. Schultz, and J. Ashton-Miller, "Stepping Responses of Young and Old Adults to Postural Disturbances: Kinematics," *Journal of the American Geriatrics Society*, vol. 42, no. 5, pp. 506–512, 1994. [Online]. Available: http://doi.wiley.com/10.1111/j.1532-5415.1994.tb04972.x
- [14] M. Vlutters, E. H. F. van Asseldonk, and H. van der Kooij, "Center of mass velocity-based predictions in balance recovery following pelvis perturbations during human walking," *The Journal of Experimental Biology*, vol. 219, no. 10, pp. 1514–1523, 2016. [Online]. Available: http://jeb.biologists.org/lookup/doi/10.1242/jeb.129338
- [15] A. L. Hof, S. M. Vermerris, and W. A. Gjaltema, "Balance responses to lateral perturbations in human treadmill walking," *Journal of Experimental Biology*, vol. 213, no. 15, pp. 2655–2664, 2010. [Online]. Available: http://jeb.biologists.org/cgi/doi/10.1242/jeb. 042572
- [16] Z. Matjačić, M. Voigt, D. Popović, and T. Sinkjær, "Functional postural responses after perturbations in multiple directions in a standing man: A principle of decoupled control," *Journal of Biomechanics*, vol. 34, no. 2, pp. 187–196, 2001. [Online]. Available: https://linkinghub.elsevier.com/retrieve/pii/S0021929000001822
- [17] L. A. Brown and J. S. Frank, "Postural compensations to the potential consequences of instability: Kinematics," *Gait & Posture*, vol. 6, no. 2, pp. 89–97, 1997. [Online]. Available: https://linkinghub.elsevier.com/retrieve/pii/S096663629601106X

- [18] A. Wing, S. Clapp, and R. Burgess-Limerick, "Standing stability in the frontal plane determined by lateral forces applied to the hip," *Gait & Posture*, vol. 3, no. 1, pp. 38–42, 1995. [Online]. Available: https://linkinghub.elsevier.com/retrieve/pii/0966636295908075
- [19] G. Brown, M. M. Wu, F. C. Huang, and K. E. Gordon, "Move-ment augmentation to evaluate human control of locomotor stability," *Proceedings of the Annual International Conference of the IEEE Engineering in Medicine and Biology Society, EMBS*, pp. 66–69, 2017.
- [20] V. Vashista, X. Jin, and S. K. Agrawal, "Active Tethered Pelvic Assist Device (A-TPAD) to study force adaptation in human walking," *Proceedings - IEEE International Conference on Robotics and Automation*, pp. 718–723, 2014.
- [21] S. M. Bruijn, O. G. Meijer, P. J. Beek, and J. H. van Dieen, "The effects of arm swing on human gait stability," *Journal of Experimental Biology*, vol. 213, no. 23, pp. 3945–3952, 2010. [Online]. Available: http://jeb.biologists.org/cgi/doi/10.1242/jeb.045112
- [22] P. E. Pidcoe and M. W. Rogers, "A closed-loop stepper motor waist-pull system for inducing protective stepping in humans," *Journal of Biomechanics*, vol. 31, no. 4, pp. 377–381, 1998. [Online]. Available: https://linkinghub.elsevier.com/retrieve/pii/S0021929098000177
- [23] J. F. Yang, D. A. Winter, and R. P. Wells, "Postural dynamics of walking in humans," *Biological Cybernetics*, vol. 62, no. 4, pp. 321–330, 1990. [Online]. Available: http://link.springer.com/10.1007/ BF00201446
- [24] D. Frzovic, M. E. Morris, and L. Vowels, "Clinical tests of standing balance: Performance of persons with multiple sclerosis," *Archives* of *Physical Medicine and Rehabilitation*, vol. 81, no. 2, pp. 215 – 221, 2000. [Online]. Available: http://www.sciencedirect.com/science/ article/pii/S0003999300901448
- [25] V. Joshi and M. Srinivasan, "A controller for walking derived from how humans recover from perturbations," *Journal of The Royal Society Interface*, vol. 16, no. 157, p. 20190027, 2019. [Online]. Available: https://royalsocietypublishing.org/doi/abs/10.1098/rsif.2019.0027
- [26] Y. Q. Chen and K. L. Moore, "An optimal design of pd-type iterative learning control with monotonic convergence," in *Proceedings of the IEEE Internatinal Symposium on Intelligent Control*, 2002, pp. 55–60.